REPORT DOCUMENTATION PAGE

Form Approved
OMB No. 0704-0188

1. REPORT DATE *(DD-MM-YYYY)*	**2. REPORT TYPE**	**3. DATES COVERED** *(From - To)*
July 2012	Viewgraph	July 2012- September 2012

4. TITLE AND SUBTITLE
Geometry Effects on Steady and Acoustically Forced Shear-Coaxial Jet Sprays

5a. CONTRACT NUMBER
In-House

5b. GRANT NUMBER

5c. PROGRAM ELEMENT NUMBER

6. AUTHOR(S)

Sophonias Teshome, Ivett Leyva, Juan Rodriguez, Doug Talley

5d. PROJECT NUMBER

5e. TASK NUMBER

5f. WORK UNIT NUMBER
23080533

7. PERFORMING ORGANIZATION NAME(S) AND ADDRESS(ES)

Air Force Research Laboratory (AFMC)
AFRL/RQRC
10 E. Saturn Blvd.
Edwards AFB CA 93524-7680

8. PERFORMING ORGANIZATION REPORT NO.

9. SPONSORING / MONITORING AGENCY NAME(S) AND ADDRESS(ES)
Air Force Research Laboratory (AFMC)
AFRL/RQR
5 Pollux Drive
Edwards AFB CA 93524-7048

10. SPONSOR/MONITOR'S ACRONYM(S)

11. SPONSOR/MONITOR'S REPORT NUMBER(S)
AFRL-RQ-ED-VG-2012-261

12. DISTRIBUTION / AVAILABILITY STATEMENT
Distribution A: Approved for Public Release; Distribution Unlimited. PA#12683

13. SUPPLEMENTARY NOTES
Conference paper for the 12th International Conference on Liquid Atomization and Spray Systems, Heidelberg, Germany in 1-6 September 2012.

14. ABSTRACT

This experimental study investigated the mixing behavior and characteristics of dynamic flow structures of cryogenic, non-reactive shear-coaxial jet sprays under varying flow conditions, with and without the presence of pressure perturbations due to acoustic forcing transverse to the flow direction. The role of injector geometry was examined using shear-coaxial injectors with different outer-to-inner jet area ratios and different inner jet post thickness to inner jet diameter ratios. Flow conditions spanning a high pressure spray (reduced pressure of 0.44) ranging up into the supercritical regime (reduced pressure of 1.05), with varying outer-to-inner jet momentum flux ratios (0.5 – 20), and maximum or minimum amplitude in the pressure perturbation at the jet axis location were considered. Nitrogen was used as the test fluid. The inner and outer jet temperatures were independently controlled so that the inner condensed flow was cooled down to below saturation temperature of the liquid, and to below the critical temperature for the supercritical fluid. Back-lighting the coaxial spray/supercritical jet resulted in a silhouette of the dense inner core, which appeared as a dark column. This distinguished it from the outer gaseous flow, and thus, enabled high speed images to capture the jet flow dynamics. Dark-core, pertaining to the unmixed portion of the dense inner flow, and length measurements were used to indicate the extent of mixing under the different flow conditions and injector geometries. As expected, increasing the momentum flux ratio resulted in shorter dark-core lengths. However, the extent of influence of momentum flux ratio was dependent on the injector geometry, whereby, the dark-core length of a large outer-to-inner jet area ratio injector flow was more influenced by increasing momentum flux ratios. A small area ratio injector flow, on the other hand, showed a more gradual decrease in its dark-core length with increasing momentum flux ratios. A basic application of proper orthogonal decomposition on the intensity fluctuation of the high-speed images enabled the extraction of the spatial and temporal characteristics of the dominant flow structures that existed in the flow field during exposure to acoustic forcing. Regardless of injector geometry or pressure regime, lower momentum flux ratio (generally less than 5) flows were found to be responsive to acoustic forcing. With increasing momentum flux ratio, however, and their corresponding acoustically forced flows revealed that, for a large-area ratio injector flow with high momentum flux ratio (generally more than 10), the baseline flow behavior was retained in the forced flow, thereby indicating a flow regime that was less sensitive to external pressure disturbances.

15. SUBJECT TERMS

16. SECURITY CLASSIFICATION OF:			**17. LIMITATION OF ABSTRACT**	**18. NUMBER OF PAGES**	**19a. NAME OF RESPONSIBLE PERSON**
					Doug Talley
a. REPORT	**b. ABSTRACT**	**c. THIS PAGE**	SAR	26	**19b. TELEPHONE NO** *(include area code)*
Unclassified	**Unclassified**	**Unclassified**			661-275-6174

Standard Form 298 (Rev. 8-98)
Prescribed by ANSI Std. 239.18

Geometry Effects on Steady and Acoustically Forced Shear-Coaxial Jet Sprays

Sophonias Teshome†, Ivett A. Leyva‡, Juan I. Rodriguez‡, Douglas Talley‡

†University of California, Los Angeles

‡Edwards AFRL

ICLASS

12th Triennial International Conference on

Liquid Atomization and Spray Systems, Heidelberg, Germany

September 2012

Motivation

- Feedback cycle between liquid rocket engine (LRE) combustion chamber pressure perturbations and unsteady combustion[1,2]
- Large amplitude fluctuations in pressure and combustion heat release rates ⇒ combustion instability

[1]Harrje, D.T., and Reardon, F.H.. *Scientific and Technical Information Office*, National Aeronautics and Space Administration, NASA SP-194, 1972.

[2]Schadow, K.C., Gutmark, E., Parr, T.P., Parr, D.M., Wilson, K.J., and Crump, J.H.. *19th AIAA Fluid Dynamics, Plasma Dynamics and Lasers Conference*, AIAA 1987-1326

Motivation (cont'd)

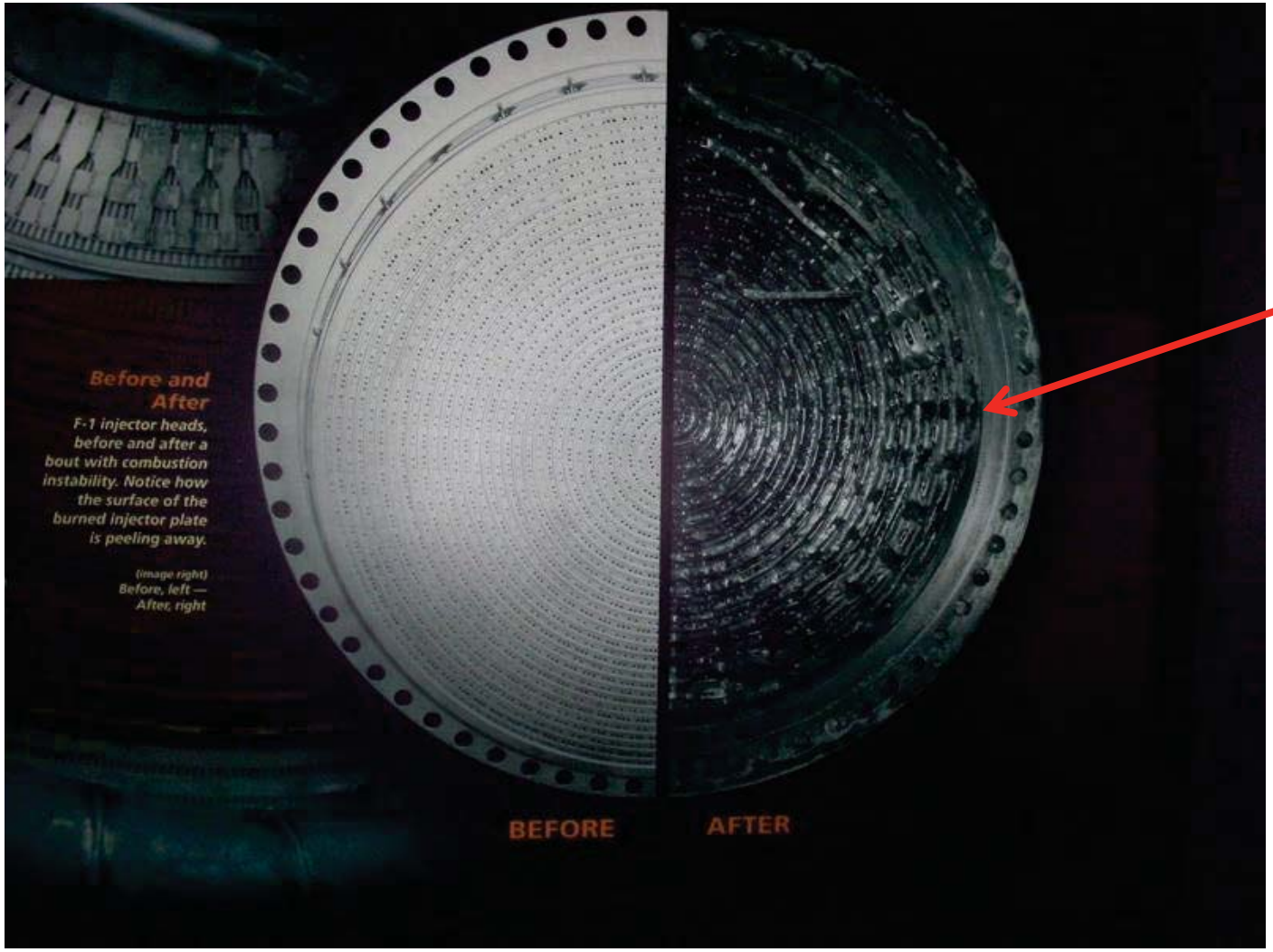

Injector head molten after a combustion instability event

Courtesy: U.S. Rocket and Space Center, Huntsville, AL

Objective

- Impose external acoustic perturbations, and examine the response and stability characteristic of shear-coaxial injector flow to pressure perturbation

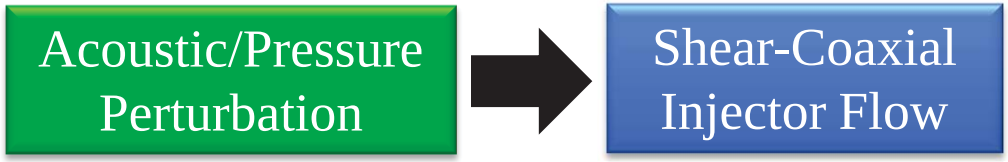

- Investigate influence of injector geometry on flow response to external pressure perturbation
- Vary the outer-to-inner jet momentum flux ratio, *J*, under subcritical chamber pressure condition, i.e., reduced pressure *Pr* = 0.44

$$J = \frac{\rho_o u_o^2}{\rho_i u_i^2} \qquad Pr = \frac{P_{chamber}}{P_{critical,\mathrm{N}_2}} \qquad P_{critical,\mathrm{N}_2} = 493\,\mathrm{psi}\,(3.4\,\mathrm{MPa})$$

- Characterize mixing using dark-core length measurements
- Apply proper orthogonal decomposition of high-speed image pixel intensity fluctuations to extract spatial and temporal characteristics of prevalent coherent flow structures

Schematic of Experimental Facility

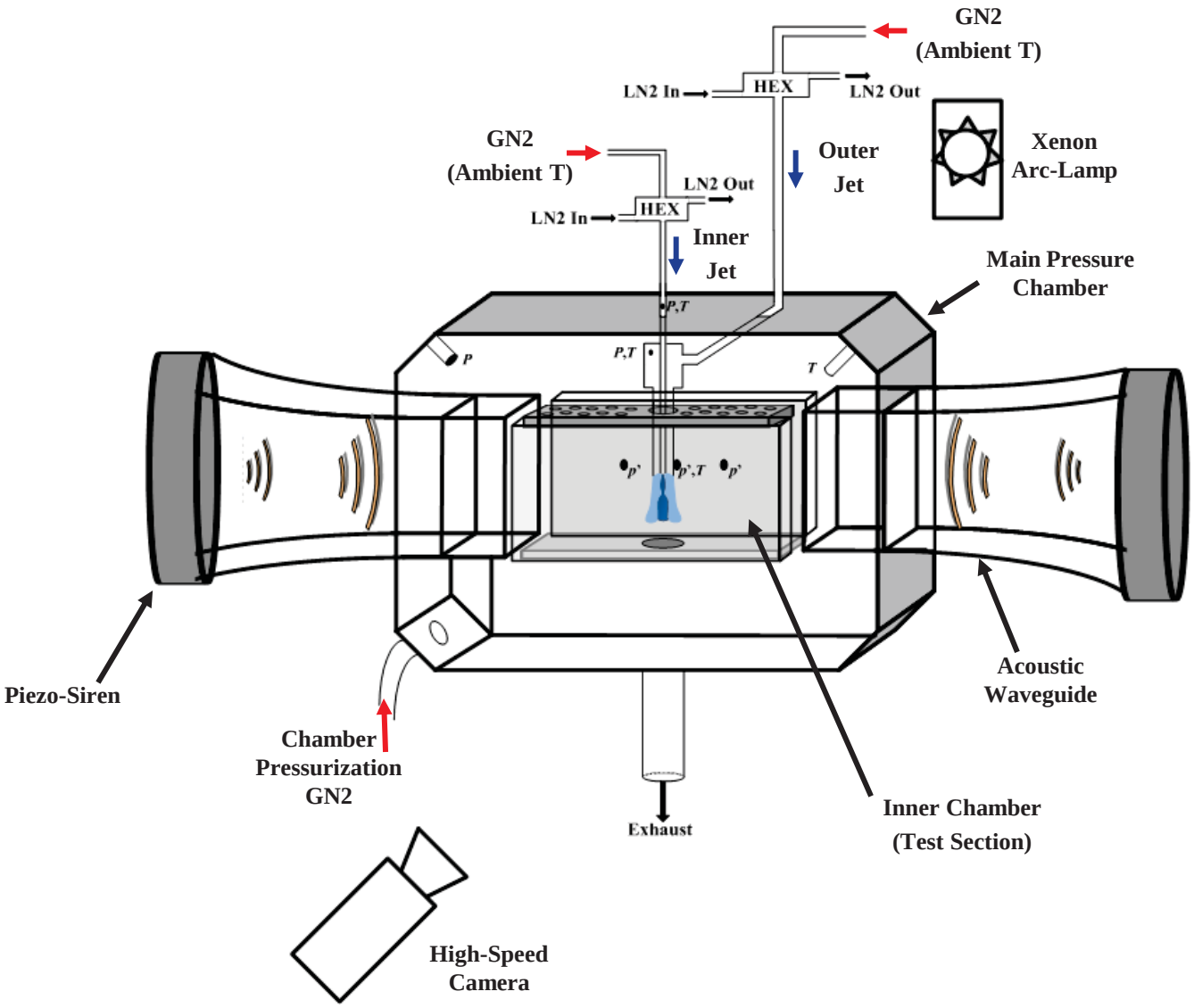

Image of Experimental Facility

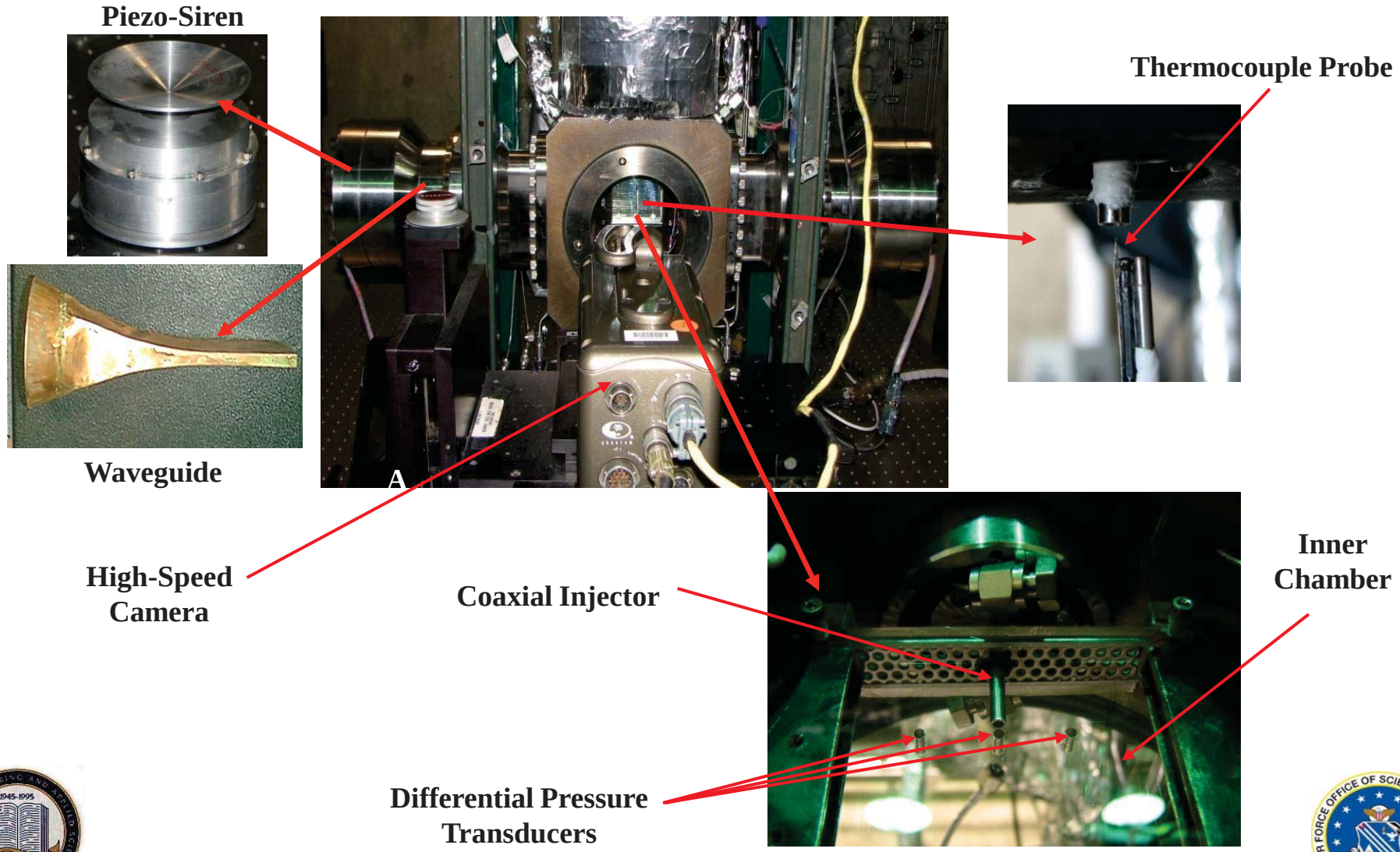

Additional Geometric Configurations

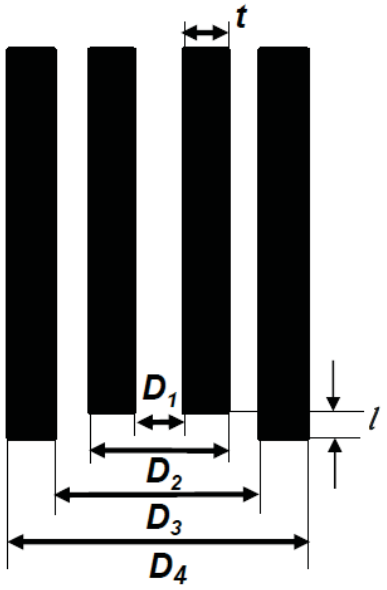

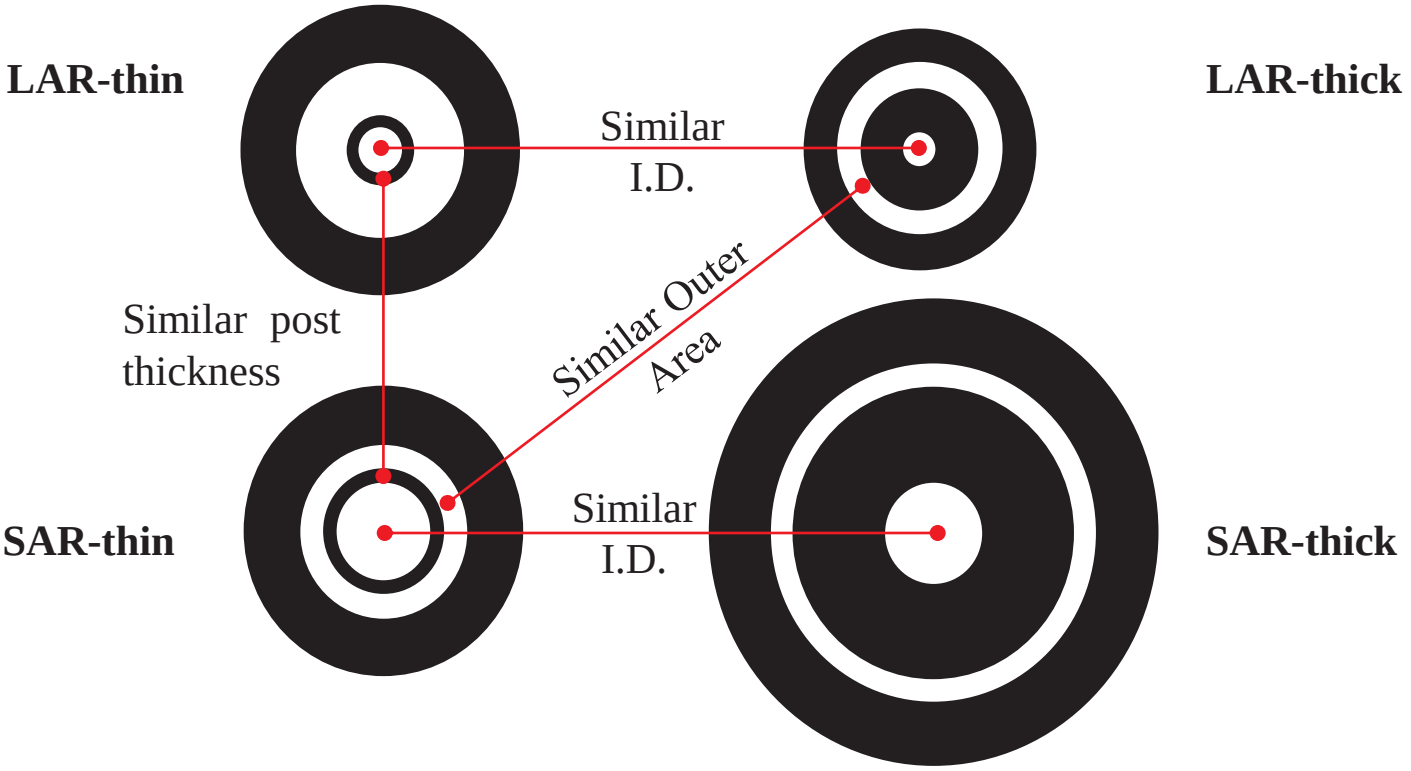

All dimensions in mm

Injector	D_1	D_2	D_3	D_4	t/D_1	A_o/A_i	l/D_1
LAR-thick	0.51	1.59	2.42	3.18	1.05	12.9	0.5
SAR-thin	1.40	1.65	2.44	3.94	0.09	1.6	0.5
SAR-thick	1.47	3.96	4.70	6.35	0.84	2.9	-0.1
LAR-thin	0.70	0.89	2.44	3.94	0.13	10.6	-0.2

SAR, LAR → Small, Large Area Ratio
Thick, Thin → Post thickness

Davis, Rodriguez, Leyva *et al.*

Rodriguez, Graham *et al.* ($l/D_1 = 0$)

Present study (-0.11 D_1 recess)

Present study (-0.21 D_1 recess)

Acoustic Field Set-Up: Pressure Antinode

- Pressure antinode (PAN) – condition of maximum pressure perturbation in the acoustic field
- Piezo-sirens forced in-phase
- Superposition of quasi-1D acoustic waves traveling in opposite directions ⇒ PAN at the jet location (geometric center of test section)

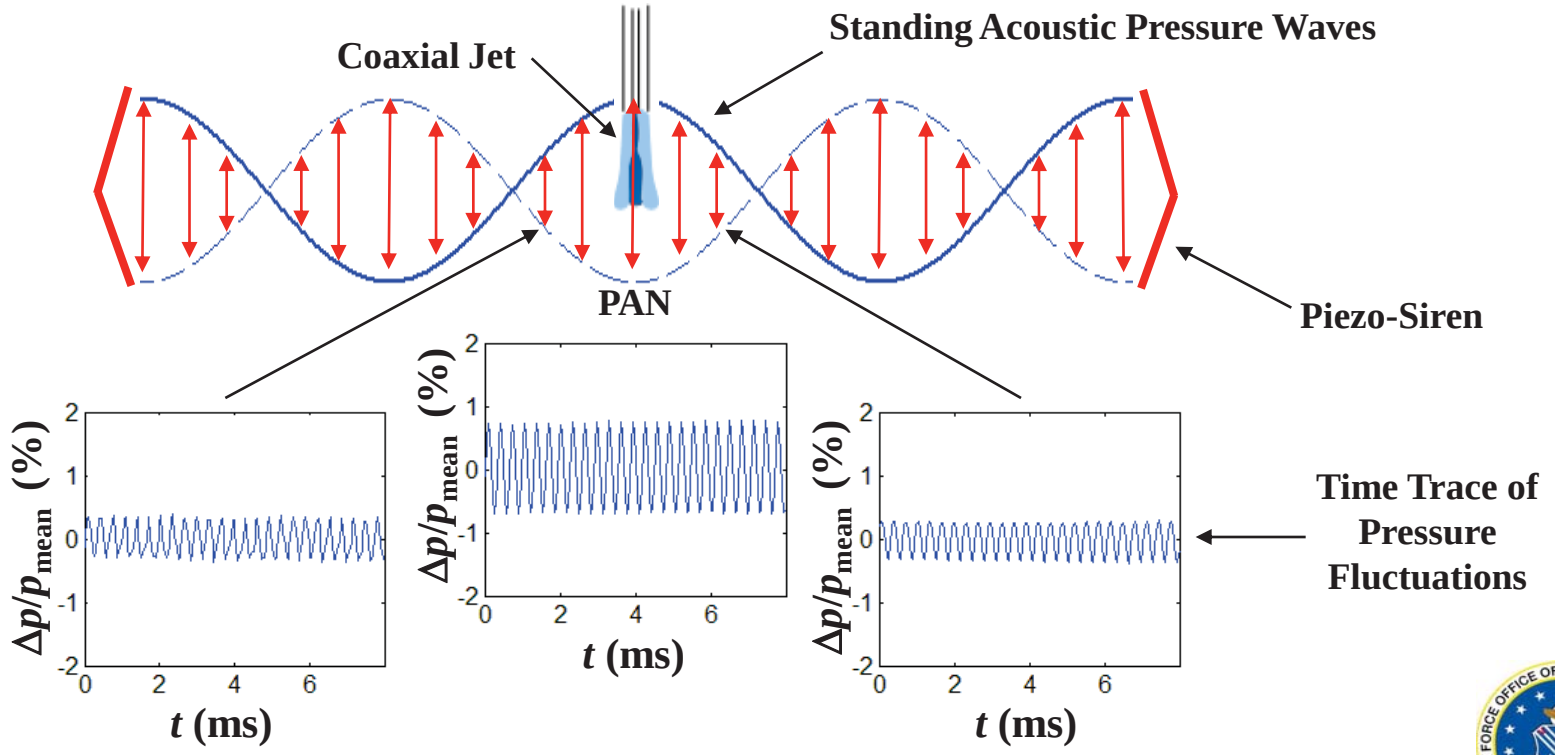

Dark-Core Length Measurement

- First raw grayscale images were converted to binary images
- A contour was drawn around the "dark-column" in the binary image
- Axial length of the dark-column measured and defined as the Dark-Core Length, *L*

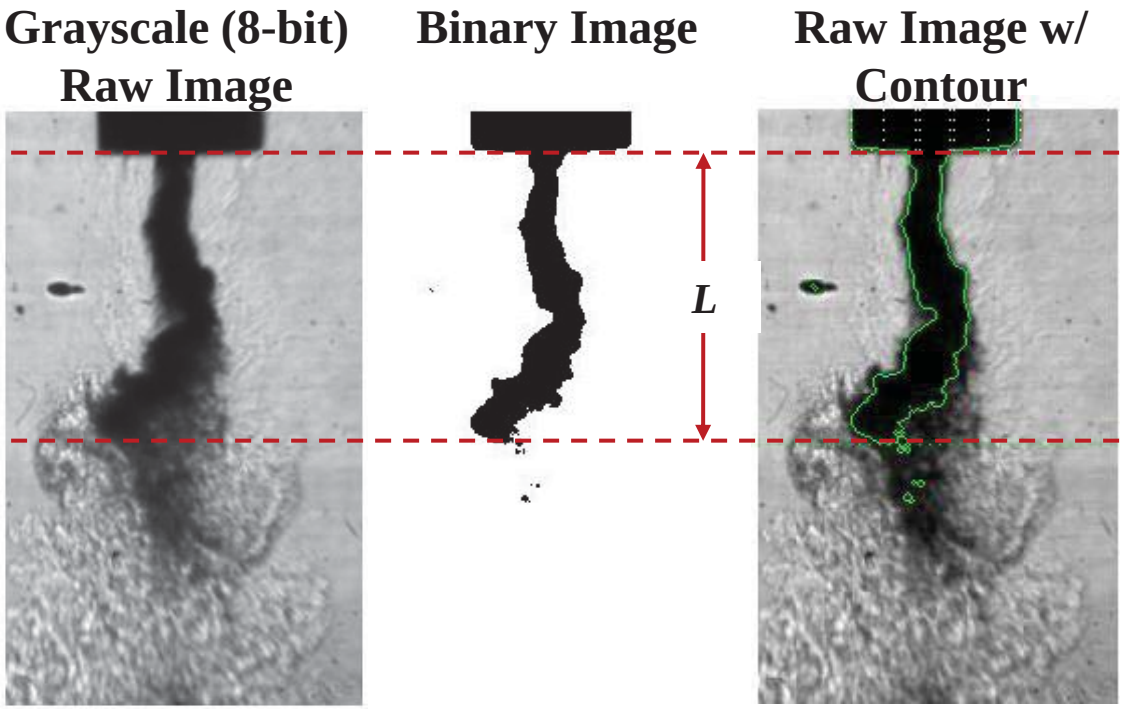

Baseline Dark-Core Lengths

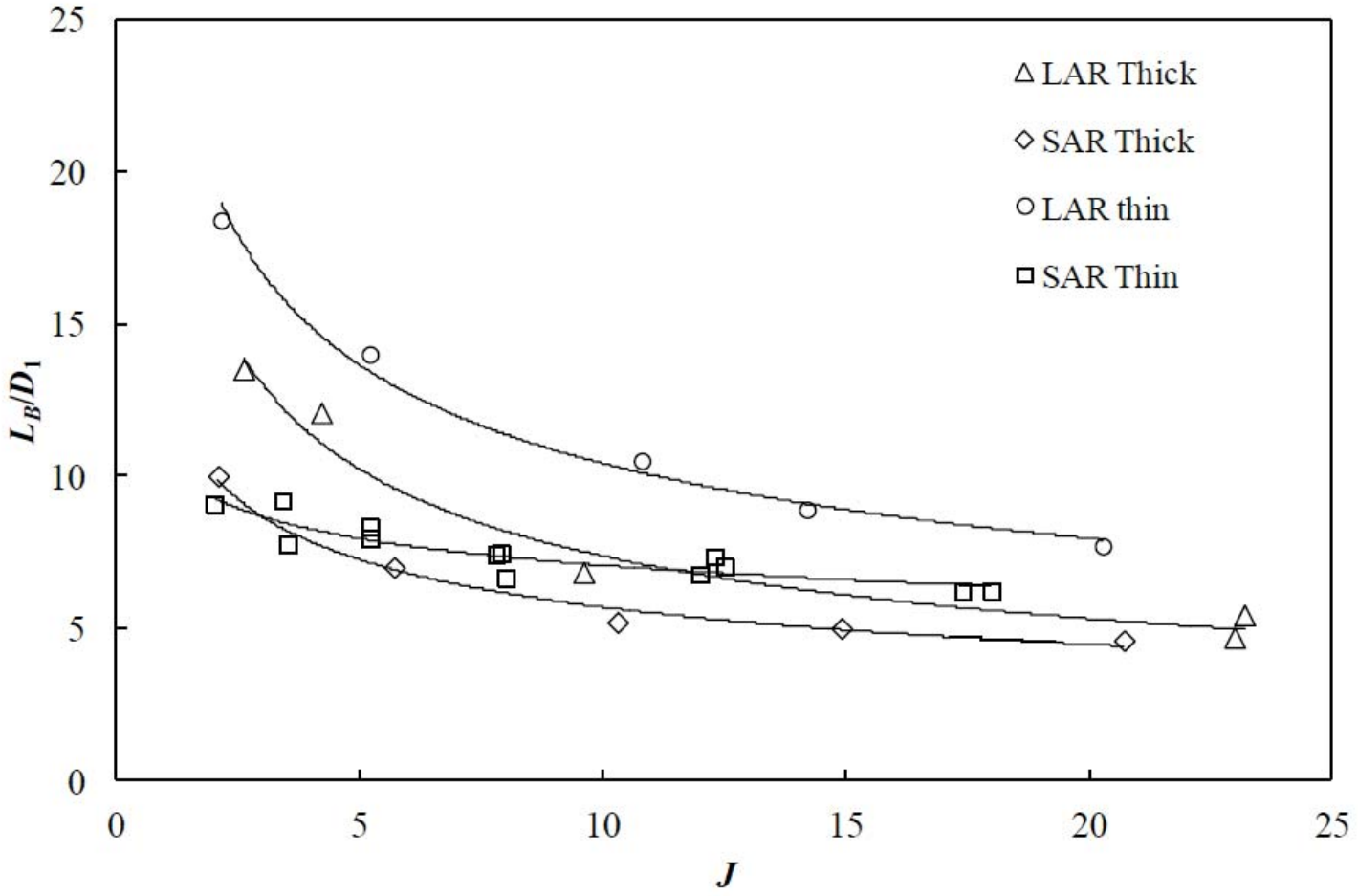

Proper Orthogonal Decomposition

• Proper Orthogonal Decomposition (POD) or Principal Component Analysis (PCA) was used for extracting dominant dynamical processes embedded in high-speed images.

• A time-resolved set of images $A(x,t)$ can be represented as a linear combination of orthonormal basis functions ϕ_k (aka proper orthogonal modes)[1,2,3] :

$$A(x,t) = \sum_{k=1}^{M} a_k(t)\phi_k(x)$$

where $a_k(t)$ are time dependent orthonormal amplitude coefficients and M is the number of modes

• Main idea: POD modal amplitudes capture the maximum possible "energy" in an average sense[4], i.e.,

$$\sum_k \langle a_k(t)a_k(t)\rangle \geq \sum_k \langle b_k(t)b_k(t)\rangle$$

where $b_k(t)$ are the temporal coefficients of a decomposition with respect to an arbitrary orthonormal basis ψ_k.

[1] **Chatterjee, A**. *Current Science*, Vol. 78, No. 7 (2000)
[2] **Arienti, M, and Soteriou, M.C.**. Phys. Fluids 21, 112104 (2009)
[3] **Narayanan,V., Lightfoot, M.D.A, Schumaker, S.A., Danczyk, S.A.,** and **Eilers, B.**. *ILASS Americas,* 2011
[4] **Berkooz, G., Holmes, P., and Lumley, J.L.**. *Annu. Rev. Fluid Mech.* 25. 539 (1993)

Construction of Data Set

• First, form a row vector consisting of all pixel intensity values of each snapshot image (with resolution of *n* rows by *m* columns) in order of increasing columns, then increasing rows

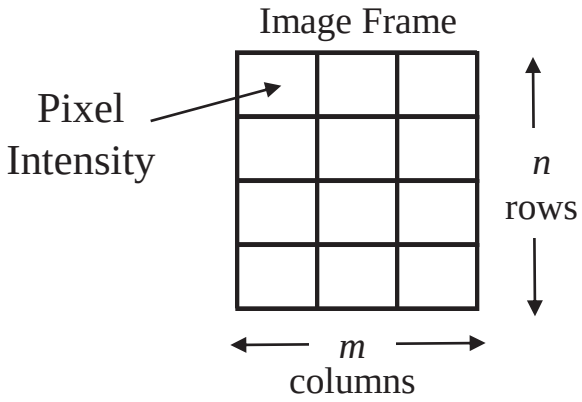

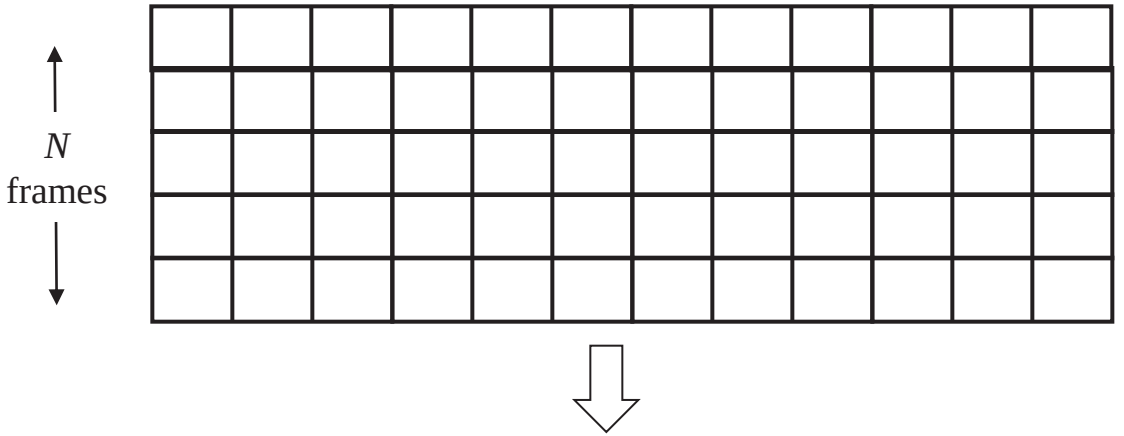

• Then, combine all such row vectors for *N* sequences of image frames resulting in a matrix **A** consisting of *N* rows by $P = n \times m$ columns of intensity values.

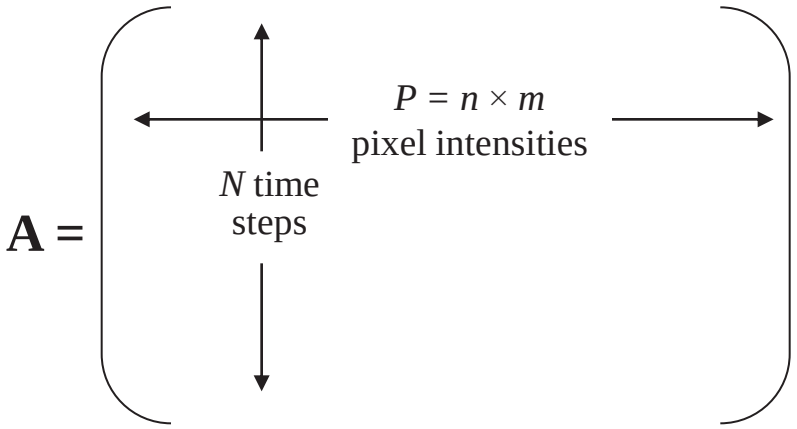

Orthogonal Decomposition Technique

- Eigenvalue decomposition or singular value decomposition (SVD) can be used
- SVD preferred since
  1. Applicable to non-square matrices (most likely the case)
  2. Decomposition matrices are orthogonal
  3. Subroutine readily available in MATLAB®
- Subtracted temporal mean of $\mathbf{A} \Rightarrow$ matrix of intensity fluctuations $\tilde{\mathbf{A}}$
- Applied SVD

$$\Rightarrow \tilde{\mathbf{A}} = \mathbf{U}\mathbf{S}\mathbf{V}^{\mathrm{T}} = \mathbf{Q}\mathbf{V}^{\mathrm{T}}$$

Columns of $\mathbf{Q} \sim a_k(t)$ contain temporal information

Columns of $\mathbf{V} \sim \phi_k(x)$ contain spatial information

$N \times N$

Orthogonal Matrix of Left Singular Column Vectors of $\tilde{\mathbf{A}}$

$N \times P$

Orthogonal Matrix of Right Singular Column Vectors of $\tilde{\mathbf{A}} \Leftrightarrow$ proper orthogonal modes (POM)

$N \times N$

Diagonal Matrix of Singular Values

Results – Subcritical Baseline at Low *J*

- LAR, *Pr* = 0.44, *J* = 0.5

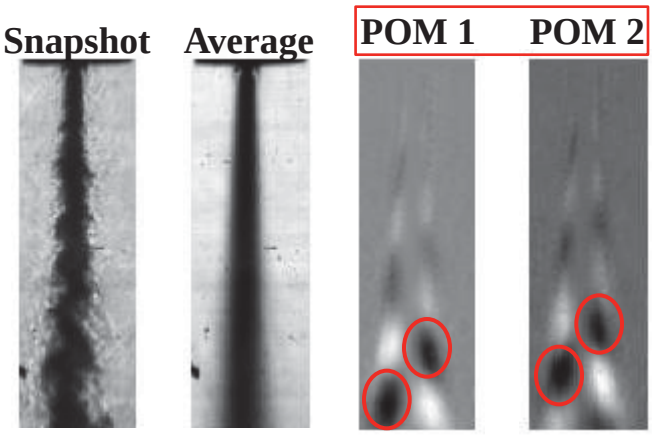

Amplitude information contained in singular values

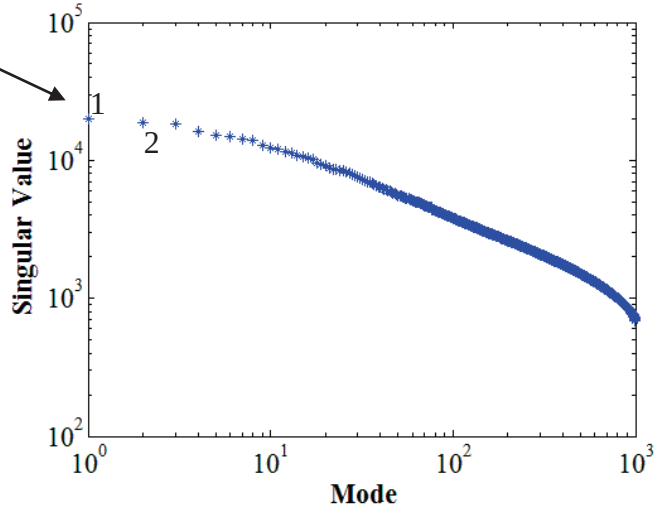

Antisymmetric Structures Identified with Characteristic Frequencies

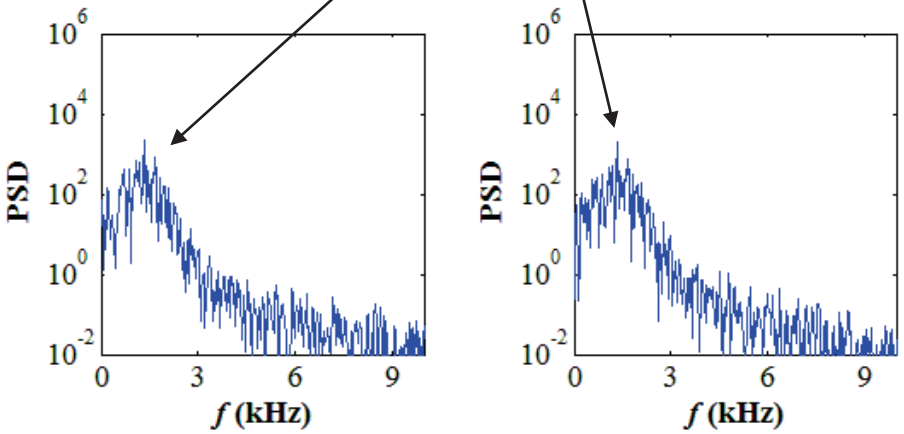

Power Spectral Densities (PSD) of Temporal Coefficients of POMs 1 and 2

Results – Subcritical PAN at Low *J*

- LAR, $Pr = 0.44$, $J = 0.5$, forcing Frequency, $f_F = 3.14$ kHz

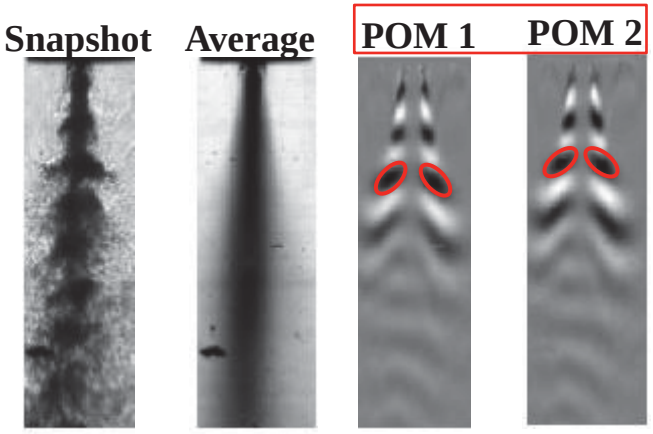

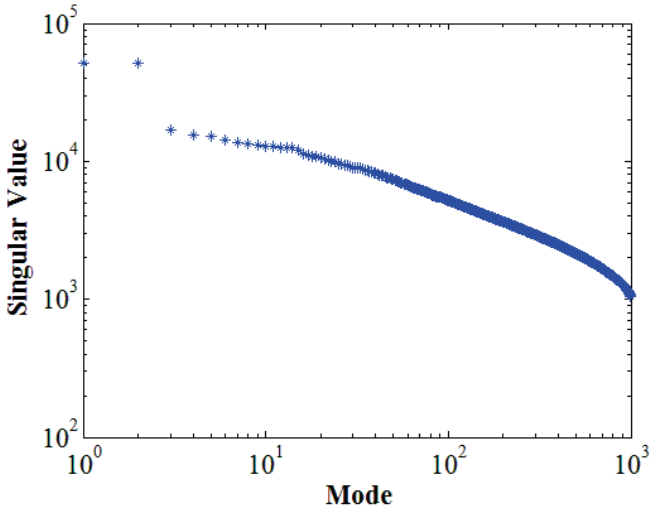

Symmetric Structures
Identified with Characteristic Frequency at f_F

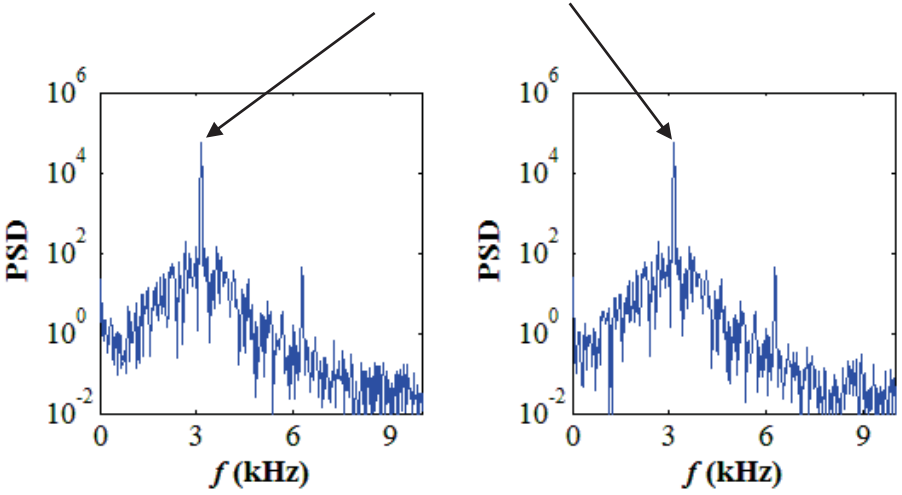

Cross-Power Spectral Density (CPSD)

- CPSD yields the FFT of the cross-correlation of the temporal coefficients

$$\mathrm{CPSD} = \sum_{k=0}^{N-1} \frac{\mathrm{cov}(a_x, a_y)}{\sigma_{a_x}\sigma_{a_y}} e^{-i\omega k}$$

- Magnitude and phase plots used to determine existence of propagating structures

LAR, $Pr = 0.44$, $J = 0.5$

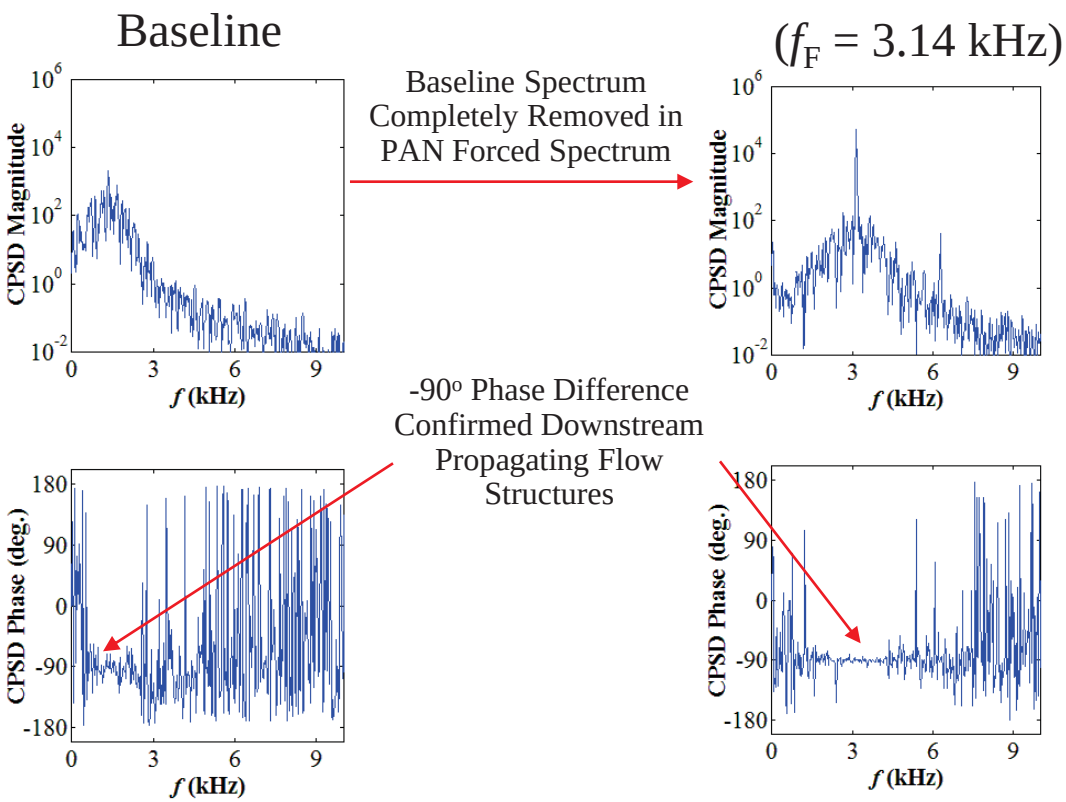

Sample Animation – PAN (f_F = 3.14 kHz)

- LAR Pr = 0.44, J = 0.5

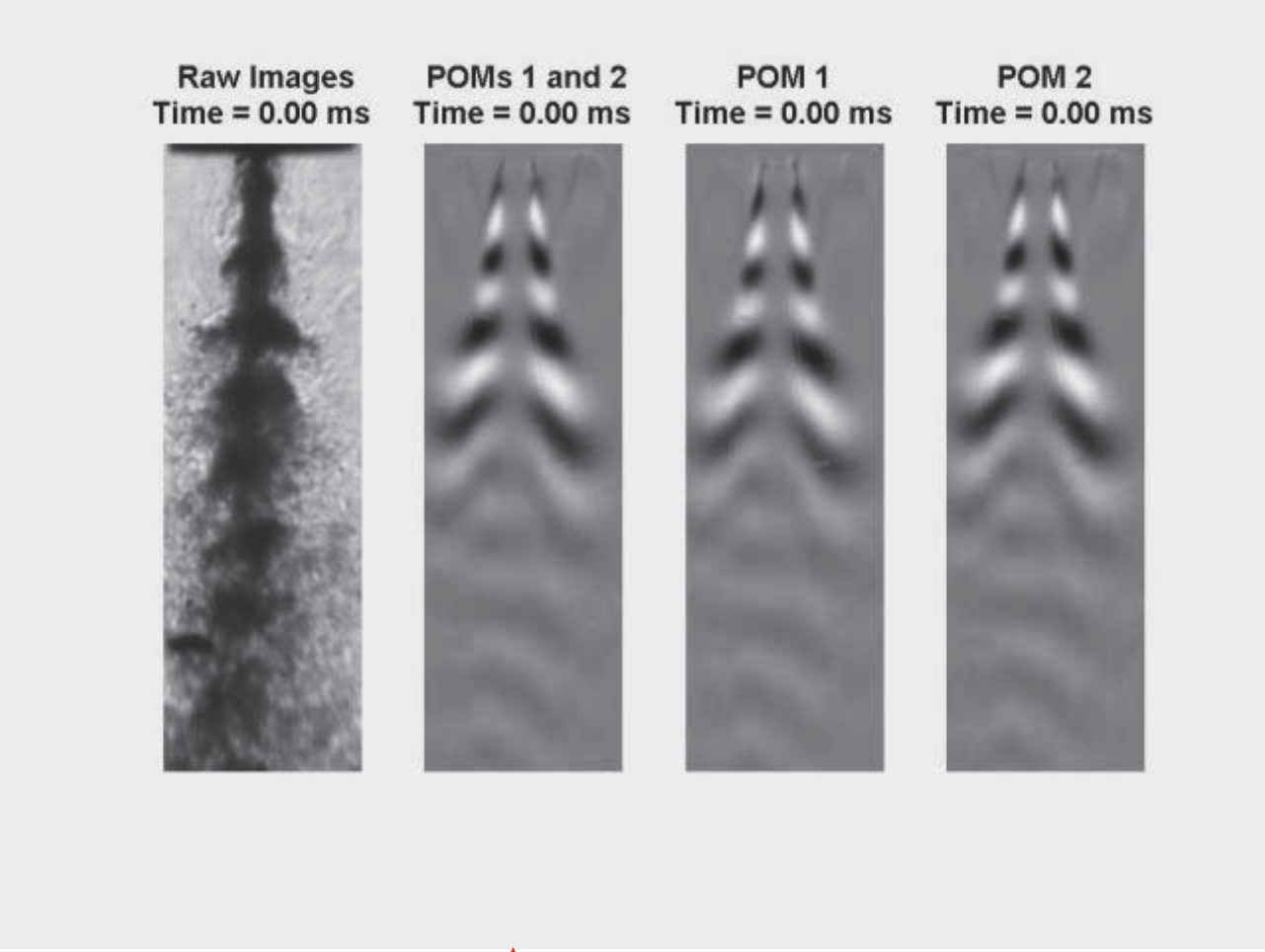

Superposition of POMs 1 and 2 Resulted in Downstream Propagating Structures

Results – LAR-thin

- Antisymmetric flow structures indicated helical type flow instabilities for all J

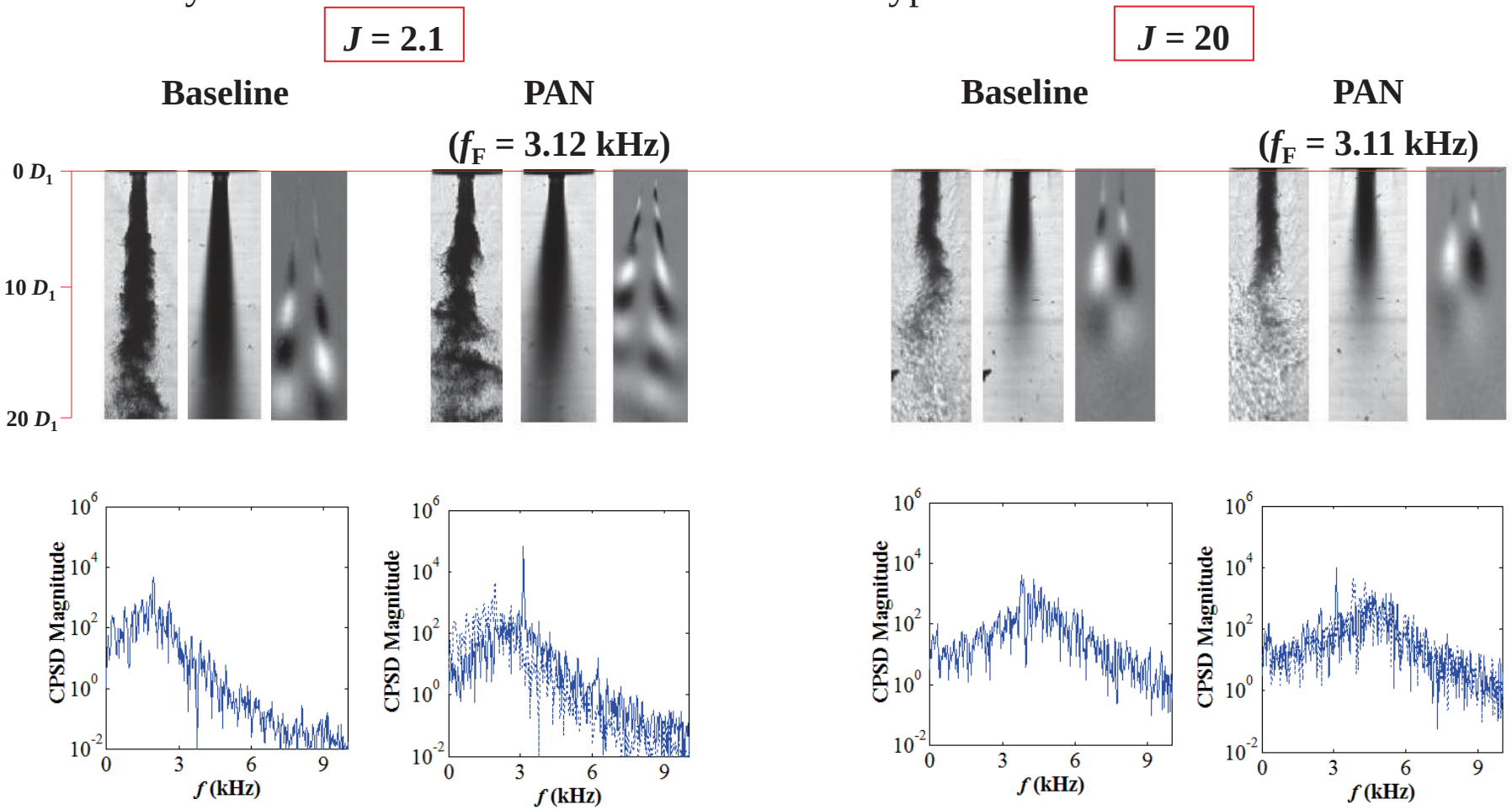

Previous Works on Jet Instability

- Michalke and Hermann (1982) did linear, inviscid instability analysis of a circular jet with coflow
- Showed that with increasing coflow velocity, U_∞
  - Helical disturbances more unstable than axisymmetric ones farther downstream of exit
  - Jet flow becomes less unstable, but spectrum of spatial growth rate becomes broader and the peak shifts to higher frequencies

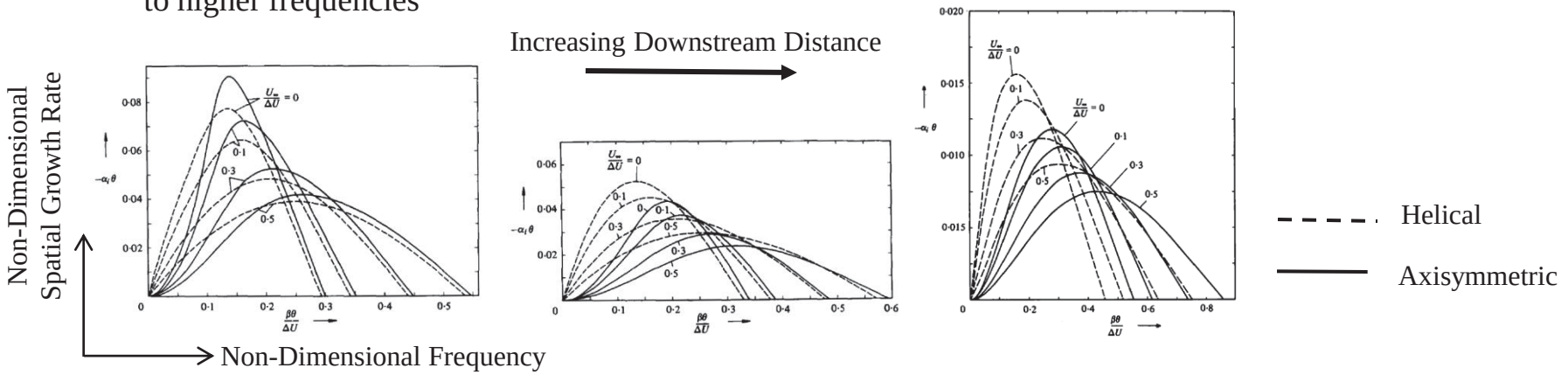

- Dahm *et al.* (1992), Wicker and Eaton (1994) conducted experimental investigation of large-scale vortex structures in the near field of coaxial jets
  - For outer-to-inner jet velocity ratios greater than one, found that coherent structures in the outer shear layer dominate those in the inner shear layer
  - At large axial distances, shear-layer vortices exhibit helical structures

Dahm *et al.*, *JFM* 1992

Results – SAR-thin

- Helical type flow instabilities became more well-defined with increasing J

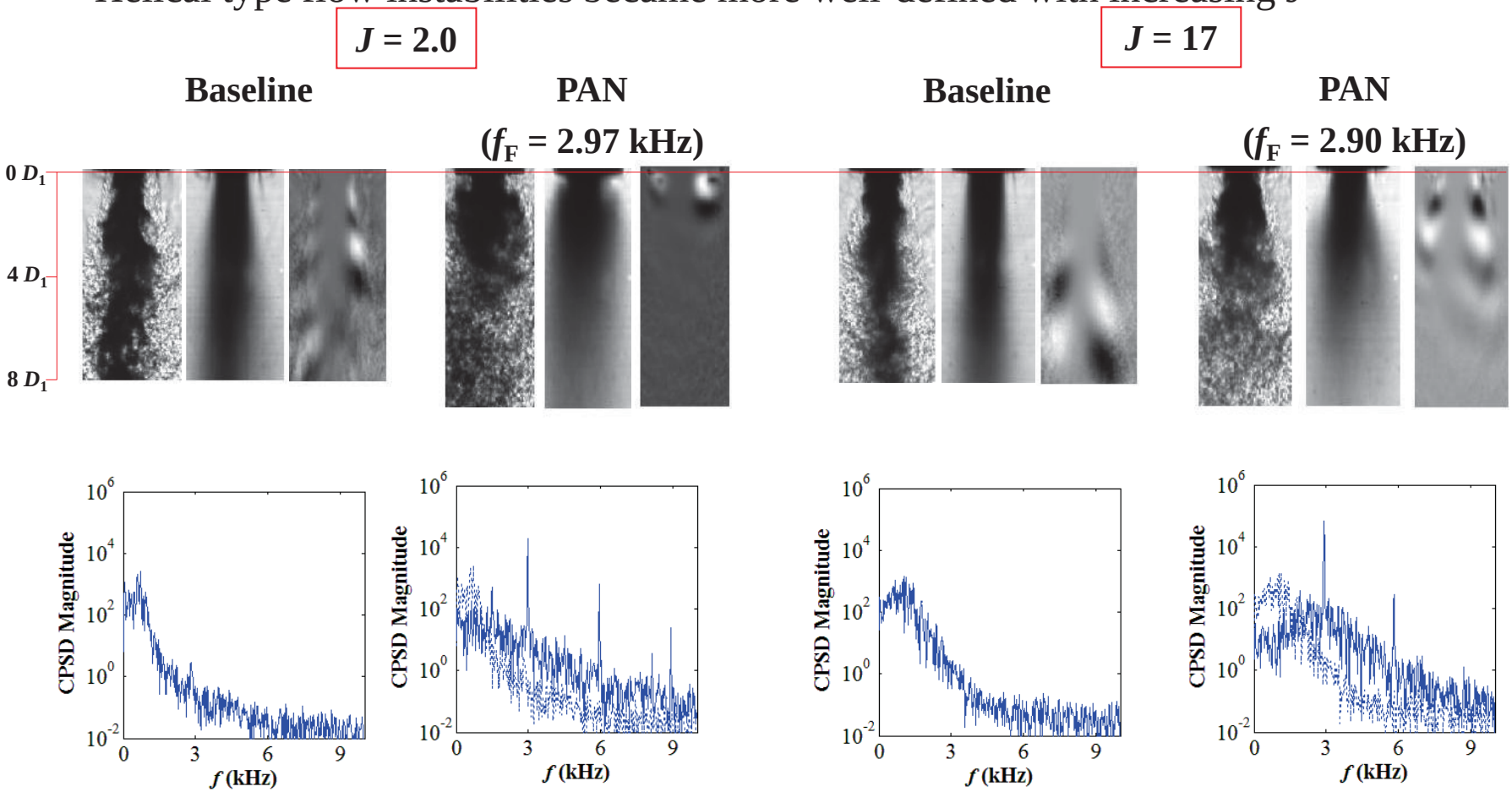

Results – SAR-thick

- Helical type flow instabilities became more well-defined with increasing J

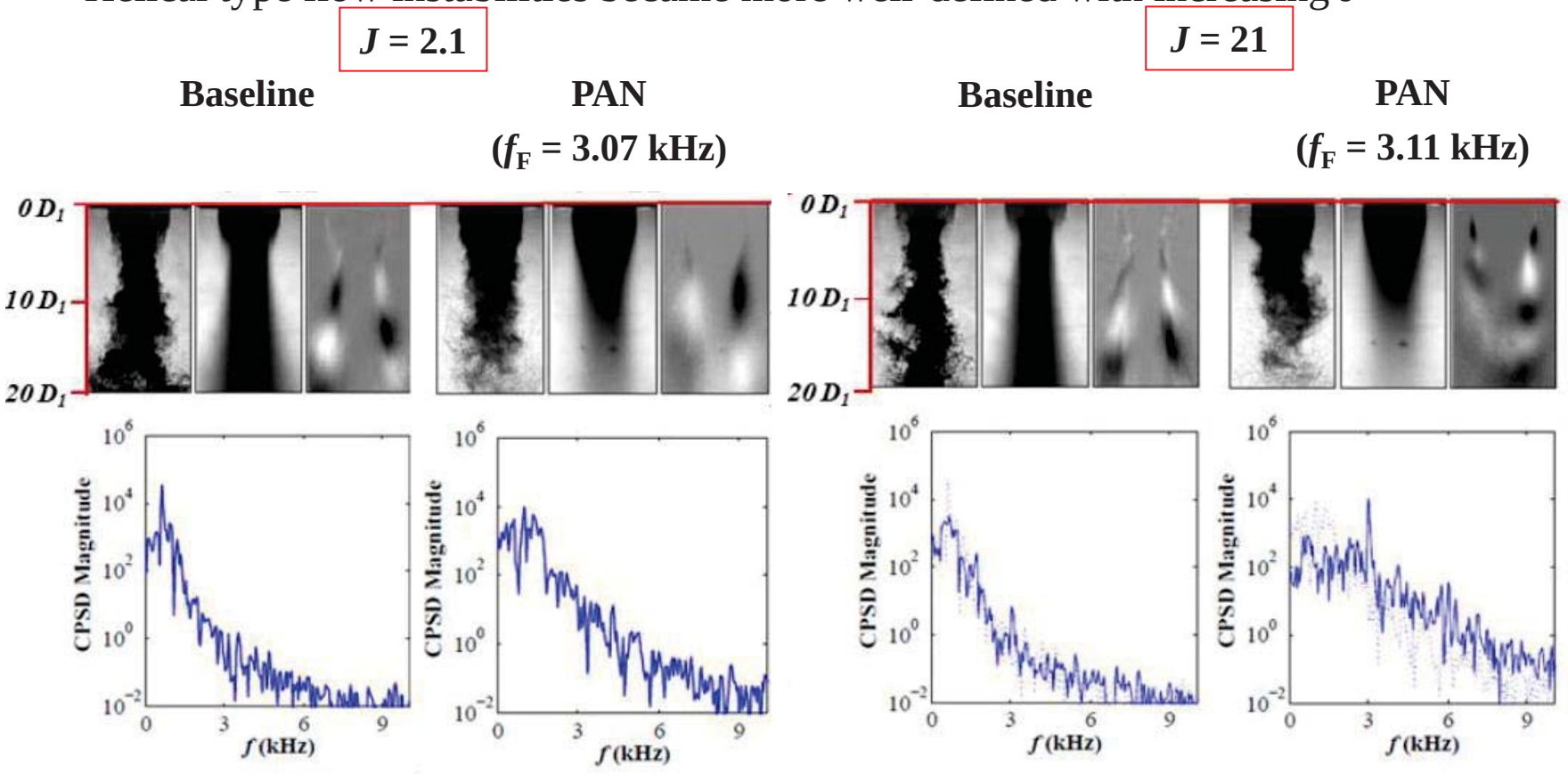

Summary and Conclusions

- Examined the effect of different exit geometries on the mixing characteristics as well as the behavior of flow disturbance structures with and without transverse acoustic forcing -- ***mixing not only depends on momentum flux ratio!***
- Proper orthogonal decomposition of high-speed image intensity fluctuation data revealed key spatial and temporal characteristics of flow structures
- Low *J*, SAR injector flows, had significantly lower L_B/D_1 than the large area ratio flows
- Low *J* LAR-thin injector flow showed a strong response at the PAN forcing frequency while the high *J* appeared less responsive and retained the baseline flow spectral characteristic
- SAR-thin injector flow showed strong response at the PAN forcing regardless of *J*
- Low *J* SAR-thick injector flow showed no response at the forcing frequency, while the high *J* flow did
- Operated at high enough *J*, LAR injector flows less vulnerable to external pressure disturbances

Acknowledgement

- Technicians
  - Randy Harvey, David Hill, Earl Thomas (ERC)
  - Todd Newkirk (Jacobs Engineering)
- This work is sponsored by the Air Force Office of Scientific Research under Dr. Mitat Birkan, program manager.

Back-Up

Data Summary Table

Injector	*J*	*R*	T_{ch} *K*	ρ_{ch} kg/m^3	P_{ch} *MPa*	T_o *K*	$\dot{m}_o$ *mg/s*	ρ_o kg/m^3	U_o *m/s*	Re_o $x10^4$	T_i *K*	$\dot{m}_i$ *mg/s*	ρ_i kg/m^3	U_i *m/s*	Re_i $x10^4$
SAR-thin	2.0	6.9	246	21	1.49	195	450	27	6.6	1.1	109	925	630	0.96	1.5
SAR-thin	17	20	217	24	1.48	194	1300	27	19	3.1	108	925	638	0.95	1.4
LAR-thin	2.1	7.4	220	23	1.50	205	2212	25	22	6.3	107	725	646	2.9	2.1
LAR-thin	20	22	220	23	1.50	204	4633	26	45	13	110	482	622	2.0	1.6
SAR-thick	2.1	7.3	205	25	1.50	212	1789	24	15	1.9	110	2130	622	2.0	3.3
SAR-thick	21	23	196	27	1.50	206	4385	25	35	4.7	107	1658	646	1.5	2.3